Electrochimica Acta 164 (2015) 97–107

Contents lists available at ScienceDirect

Electrochimica Acta

journal homepage: www.elsevier.com/locate/electacta

A highly efficient reduced order electrochemical model for a large format $LiMn_2O_4$/Carbon polymer battery for real time applications

Yinyin Zhao, Song-Yul Choe *

Mechanical Engineering, 1418 Wiggins Hall, Auburn Univ., AL 36849, USA

ARTICLE INFO

Article history:
Received 13 January 2015
Received in revised form 19 February 2015
Accepted 21 February 2015
Available online 23 February 2015

Keywords:
Lithium ion battery
electrochemical modeling
reduced order model

ABSTRACT

Mechanisms for ion transport, diffusion and intercalation/deintercalation processes in batteries during charging and discharging are described by governing equations that consist of partial differential equations and nonlinear functions. Solving these equations numerically is computational intensive, particularly when the number of cells connected in series and parallel for high power or energy increases, whereas tolerance of errors should be kept under specified limits. Reduction of the computational time is required not only for enabling simulation of the behavior of packs, but also for development of a model capable of running in real time environments, so that new advanced estimation methods for state of charge (SOC) and state of health (SOH) can be developed.

In our previous research work, a reduced order model (ROM) was developed using different techniques including polymoninal approximation and residue grouping, which represents the physical behaviors of a battery. However, computational time has not been optimized. In this paper, methods to reduce the computational time are analyzed and employed to reduce the computational time while considering the accuracy. Apart from retaining the residue grouping method for the ion concentration in electrolyte and linearization of the Butler–Volmer equation, the Padé approximation is introduced to simplify the calculation of ion concentration in electrode particles governed by the Fick's second law. Meanwhile, discretized governing equations for potentials in electrodes and electrolytes are reduced by employing proper orthogonal decomposition (POD). In addition, expressions of the equilibrium potentials for anodes and cathodes are fitted to different order polynomials. The reduced equations are coupled to construct a single cell model for a large format lithium polymer battery that is validated against experimental data. The results show that the ROM proposed can reduce the computational time at least to one-tenth of the models developed previously, while overall accuracies can be maintained.

1. Introduction

Lithium ion batteries have been widely adopted as sources of energy storage for different power systems due to their high power and energy density and reduced manufacturing costs triggered by the growing market for electronic devices. However, improper operating conditions such as continuous overcharge or undercharge can accelerate degradation processes and lead to early failures. Model based battery management is an elegant approach that enables monitoring of battery performances such as state of charge (SOC) or state of health (SOH), which are crucial for safe operation of the battery.

The models can be classified into two categories, equivalent circuit models (ECM) and electrochemical thermal models (ETM) [1,2]. The ECM is easy to construct and fast in simulation, but cannot represent battery behavior completely [3]. Conversely, the ETM based on electrochemical kinetics, mass balance, charge conservation and thermal principles is capable of representing the battery behavior accurately and providing internal variables like ion concentrations. However it is inappropriate for implementation into microcontrollers that work in real time due to the large amount of calculations caused by numerically solving discretized partial differential equations as well as nonlinear equations. The ETM describes the charge transport phenomenon in composite electrodes and electrolyte by a set of coupled partial differential equations (PDEs). The PDEs are discretized and numerically solved in radial and through-the-plane direction using the finite element method (FEM) [4]. The resulting Full Order Model (FOM) provides high accuracy although the calculation of large amount state variables is quite time consuming. In particular, the electrodes are

* Corresponding author. Tel.: +1 334 844 3329; fax: +1 334 844 3307.
E-mail addresses: yzz0031@tigermail.auburn.edu (Y. Zhao), choe@auburn.edu (S.-Y. Choe).

http://dx.doi.org/10.1016/j.electacta.2015.02.182
0013-4686/

Nomenclature

A	sandwich area of the cell (cm^2)
a_s	specific surface area of electrode (cm^{-1})
c_s	ion concentration in electrode phase ($mol\,L^{-1}$)
c_e	ion concentration in electrolyte ($mol\,L^{-1}$)
D	diffusion coefficient ($cm^2\,s^{-1}$)
F	Faraday constant (96,487 $C\,mol^{-1}$)
I	current of the cell (A)
i	current density ($A\,cm^{-2}$)
i_0	refference exchange current density ($A\,cm^{-2}$)
J^{Li}	reaction rate ($A\,cm^{-3}$)
L	thickness of micro cell (cm)
OCV	open circuit voltage (V)
R	universal gas constant ($8.3143\,J\,mol^{-1}\,K^{-1}$)
R_s	radius of spherical electrode particle (cm)
r	coordinate along the radius of electrode particle (cm)
SOC	state of charge
SOH	state of health
SOX	SOC, SOH, SOF(state of function), etc.
T	cell temperature (K)
t	time (s)
U_{equi}	equilibrium potential (V)
x	stoichiometric number in anode
y	stoichiometric number in cathode
t_+^0	initial transference number

Greek symbols

α	transfer coefficient for an electrode reaction
δ	thickness (cm)
ε	volume fraction of a porous medium
φ	Finite element method (FEM) solution of potentials
φ_{app}	approximate solution of potentials
φ_e	potential in electrolyte phase (V)
φ_s	potential in electrode phase (V)
η	surface overpotential of electrode reaction (V)
κ	ionic conductivity of electrolyte ($S\,cm^{-1}$) or kernel of the data set
κ_D	concentration driven diffusion conductivity ($A\,cm^{-1}$)
σ	conductivity ($S\,cm^{-1}$)

Subscripts

a	anodic
c	cathodic
e	electrolyte phase
$equi$	equilibrium
max	maximum
$-$	negative electrode (anode)
$+$	positive electrode (cathode)
r	radial direction in electrode particle
s	solid phase
T	terminal
0%	0% SOC
100%	100% SOC

Superscripts

eff	effective
Li	Lithium ion

modeled with spherical particles, and the evaluation of ion concentrations in the particles should be carried out in the sphere radial direction that requires an extra discretization, which multiplies the number of state variables as well as the computational time.

Models for real-time control purpose should be able to represent key physical phenomena within a reasonable time given by the implementation. Therefore, the ETM should be simplified while considering the accuracy and computational time. Several model order reduction techniques have been proposed in the literature to reduce computational expense. Review of the literature has shown that those methods can be sorted into two groups: one is based on numerical calculations and the other one is based on analytical expressions.

The numerical methods require discretization of the PDEs and reducing the matrix size by assorting eigenvalues of the system. A representative method is the residue grouping (RG) method that lumps states with similar eigenvalues, which reduces the order of the matrices [5]. Proper Orthogonal Decomposition (POD) technique approximates FOM behavior by a low order sub-model derived from the most significant eigenvalues of matrices [6].

The analytical methods are replacements of the PDE for the Fick's second law that describes the ion diffusion process that takes place in electrode particles. One of the analytical approaches employed a parabolic profile based on volume average equation [7]. Accuracy is further improved using a quartic profile instead [8]. Another analytical approach eliminated the independent spatial variables in the diffusion equation by applying the pseudo steady state (PSS) method, which is originated from finite integral transform techniques [9]. In addition, the Galerkin method has also been adopted to reduce the computational complexity of the ion concentration [10,11]. Furthermore, Padé approximation is applied to the transfer function between current density and ion concentrations [12], which is derived to study the diffusion impedance in spheres [13].

The two groups of approaches aforementioned have their own superiorities and limitations. The numerical methods are generally applicable for each part of the ETM and allow for systematic reduction of a model to a certain level that meets requirements for accuracy. Numerical methods have better frequency responses compared to the analytical expressions. However, the inevitable discretization increases the complexity of the algorithms. The analytical expressions describe the model dynamics as a function of time and space in an analytical closed form and avoid discretization of the PDEs. Nevertheless, those approximations usually provide less accuracy in the high frequency range and the determination of the coefficients is quite time consuming, especially in the PSS method. In spite of the fact that the Padé approximation is based on the analytical transfer function of the ion diffusion impedance, it has excellent performance in a wide frequency range because the transfer functions are exact solutions of the PDE. The features of high accuracy and efficiency enable it to be a promising replacement of the diffusion equation in electrode particles.

In our previous research work for the development of ROM, order reductions and simplifications were performed, including polynomial approximation for ion concentration in electrode particles, residue grouping (RG) for ion concentrations in electrolyte, and linearization of the Butler–Volmer equation [14]. Time analysis was carried out using the MATLAB profiler, as shown in Table 1, where the time measured in seconds indicates the

Table 1
Comparison of computational time (seconds) between FOM and previous ROM.

	FOM	Previous ROM [14]
Total	50.74	10.09
C_s	19.25	6.05
C_e	1.93	0.05
Phi	7.01	3.36
Others	22.55	0.63

calculation duration for 1 C discharge from 100% SOC to 0% SOC with a sample rate of 1 s. The calculation time for the major variables in model are listed individually, where C_s, C_e and *Phi* denote the ion concentration in electrode particles, in electrolytes, and potential in electrodes and electrolytes, respectively. ROM can reduce computational time to approximately one-fifth of FOM, whereby C_s and *Phi* remain the most time consuming parts of the calculation.

To reduce the calculation time for ion concentrations and potentials, different techniques were investigated to simplify the model. Four potential candidates for ion concentration in electrode particles governed by the Fick's law are polynomial approximation (Poly), Padé approximation (Pade), POD and Galerkin Reformulation (GR), whose performances are compared and analyzed [15]. Computational time and error of the four methods are plotted in Fig. 1, where the time denotes the simulation duration of $C_{s,surf}$ when a pulse current is applied for 1 hour while the error is the accumulated difference given by comparing them with a FEM solution.

The results of the analysis showed that the performance of the Padé approximation was superior to the other options since the calculation time remained within a reasonable tolerance and the error quickly converged to zero when the order number increased. Moreover, the approximation allowed for a systematic reduction of orders dependent upon the level of accuracy required.

On the other hand, RG is retained for ion concentration in electrolyte. The POD method as applied for reduction of large scale ODE systems is used to reduce the matrix size for potentials in electrode and electrolyte.

2. Lithium ion battery model based on electrochemical principles

A pouch type lithium ion polymer single cell is made of stacked microcells that are connected in parallel by current collectors. Due to the high conductivity of the current collectors, the lateral current flow from one microcell to another can be neglected and the potentials on current collectors for each microcell are assumed to be identical. Thus, the entire single cell can be regarded as a microcell with only a pair of current collectors. The microcell has a sandwich structure in the thickness direction that comprises of composite electrodes mixed with electrolyte and a separator in between. The composite electrodes are made of active materials, electrolytes and binders, where the particles dispersed on electrodes are modeled as uniformly distributed spheres. A schematic diagram for this cell is shown in Fig. 2, where the active material on the anode is graphite and that on the cathode is transition metal oxides.

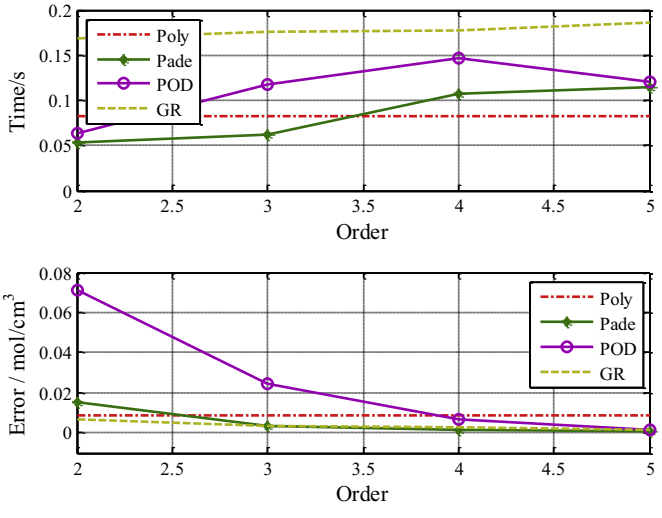

Fig. 1. Time and error analysis of four order reduction methods for ion concentration in solid.

While cells discharge or charge, ions transport through the electrolyte and react electrochemically at active materials, diffuse, and finally rest after intercalation in a lattice structure. Meanwhile, electrons flow through an external circuit and complete the redox process. The working mechanism is described by a set of coupled governing equations. The equations incorporate ion and charge conservation in electrode and electrolyte along with the Butler–Volmer equation that describes electrochemical kinetics. Four variables, including ion concentrations in the electrode and the electrolyte, and potentials in the electrode and the electrolyte, that appear in the governing equations are solved numerically using the FEM, which is called the Full Order Model (FOM). The governing equations are summarized in Table 2.

The OCV–SOC curve is obtained by pulse discharge, where terminal voltage and the SOC are measured after the battery is discharged with a small C rate for a short time and completely relaxed. The measured OCV is the difference between the equilibrium potentials for positive and negative electrode, where the potential for the negative electrode, U_-, is approximated with an empirical equation, as provided in Table 2. Then, the potential for the positive electrode, U_+, is fitted by a high order polynomial. The equilibrium potentials versus stoichiometric numbers are plotted in Fig. 3.

3. Model order reduction and simplification

Coupled governing equations consist of nonlinear equations and PDEs that are numerically solved by the FEM in FOM. The reductions and simplifications of the equations for each part of the model are described below.

3.1. Ion concentration in electrodes

Ion diffusion in a particle is described by the second order Fick's law, whose solution provides gradients of ion concentration, C_s, along the radial direction in electrode particles. For control oriented models, the ion concentration on particle surface, $C_{s,surf}$, and the volume average concentration, $C_{s,ave}$, are critical variables because of their direct relationship to the reactions that affect intercalation in active materials and SOC. Analytical solutions of the Fick's law provide two transfer functions where the current density, J^{Li}, and two ion concentrations, $C_{s,surf}$,$C_{s,ave}$, are regarded as an input variable and output variables, respectively, as shown as follows [12]:

$$\frac{C_{s,surf}(s)}{j^{Li}(s)} = \frac{1}{a_s F}\left(\frac{R_s}{D_s}\right)\left[\frac{\tanh(\beta)}{\tanh(\beta)-\beta}\right] \tag{1}$$

where $\beta = R_s\sqrt{s/D_s}$.

$$\frac{C_{s,ave}(s)}{j^{Li}(s)} = -\frac{3}{R_s a_s F s} \tag{2}$$

The Q^{th} order Padé approximation for $C_{s,surf}$ in Eq. (1) results in the form of:

$$\frac{C_{s,surf}(s)}{j^{Li}(s)} = \frac{a_0 + a_1 s + a_2 s^2 + \cdots a_{Q-1}s^{Q-1}}{s(1 + b_2 s + b_3 s^2 + \cdots b_Q s^{Q-1})} \tag{3}$$

The coefficients $a_0, a_1, \cdots, a_{Q-1}$ and $b_2, b_3, \cdots, b_Q$ are determined by comparing the derivatives of Eq. (1) with Eq. (3) at s = 0. The resulting low order Padé approximations are listed in Table 3, where $m = \frac{1}{a_s F D_s}$.

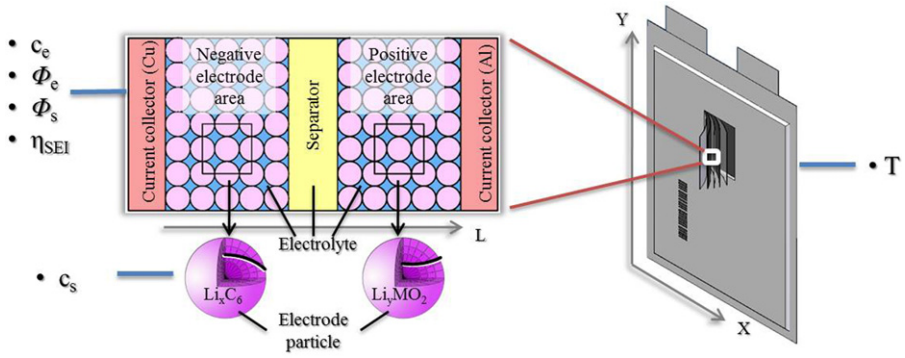

Fig. 2. Schematic diagram of a model for a pouch type single cell.

A state space representation in controllable canonical form of the transfer function in Eqs. (2) and (3) is shown as:

$$\dot{\vec{x}} = A_1\vec{x} + B_1 j^{Li} \qquad \vec{y} = C_1\vec{x} \tag{4}$$

where

$$A_1 = \begin{bmatrix} 0 & 1 & 0 & 0 & \cdots & 0 \\ 0 & 0 & 1 & 0 & \cdots & 0 \\ 0 & 0 & 0 & 1 & \cdots & 0 \\ \vdots & \vdots & \vdots & \vdots & \ddots & 0 \\ 0 & 0 & 0 & 0 & \cdots & 1 \\ 0 & -\frac{1}{b_Q} & -\frac{b_2}{b_Q} & -\frac{b_3}{b_Q} & \cdots & -\frac{b_{Q-1}}{b_Q} \end{bmatrix}, \quad B_1 = \begin{bmatrix} 0 \\ 0 \\ 0 \\ \vdots \\ 0 \\ 1 \end{bmatrix},$$

$$x = \begin{bmatrix} x_1 \\ x_2 \\ x_3 \\ \vdots \\ x_{Q-1} \\ x_Q \end{bmatrix} \quad C_1 = \begin{bmatrix} \frac{a_0}{b_Q} & \frac{a_1}{b_Q} & \frac{a_2}{b_Q} & \frac{a_3}{b_Q} & \cdots & \frac{a_{Q-1}}{b_Q} \\ \frac{a_0}{b_Q} & \frac{a_0 b_2}{b_Q} & \frac{a_0 b_3}{b_Q} & \frac{a_0 b_4}{b_Q} & \cdots & a_0 \end{bmatrix},$$

$$\vec{y} = \begin{bmatrix} C_{s,surf} \\ C_{s,ave} \end{bmatrix} \tag{5}$$

Initial conditions for solving the equations above are steady state, $\dot{x} = 0$, zero input $j^{Li} = 0$ and uniform concentration, $C_{s,surf} = C_{s,ave}$. The first two conditions result in a linear equation, $A\vec{x} = 0$, that yields a solution with one degree of freedom, $\vec{x}_0 = [x_0 \quad 0 \quad 0 \quad \cdots \quad 0 \quad 0]^T$. The third condition gives an initial value of the concentration, $C_{s,surf} = C_{s,ave} = C_{s,0}$. As a result, the initial state is presented as follows:

$$\vec{x}_0 = \begin{bmatrix} C_{s,0}\frac{b_Q}{a_0} & 0 & 0 & \cdots & 0 & 0 \end{bmatrix}^T \tag{6}$$

3.2. Ion concentration in electrolyte

The RG method is used to reduce the PDE that describes ion transport in electrolytes, where current density across each electrode is assumed to be uniform, as shown in Eq. (7):

$$\begin{aligned} j_-^{Li} &= \frac{I}{AL_-} \quad \text{(Negative electrode)} \\ j_{sep}^{Li} &= 0 \quad \text{(separator)} \\ j_+^{Li} &= -\frac{I}{AL_+} \quad \text{(Positive electrode)} \end{aligned} \tag{7}$$

The PDE is discretized by the FEM and the resulting equations are converted into the state space representation:

$$\dot{\vec{x}} = A_2\vec{x} + B_2 I \qquad y = C_2\vec{x} + D_2 I \tag{8}$$

The equation above is a single input M output linear system with matrices $A_2, B_2, C_2 \text{and} D_2$ that have dimensions of $M \times M, M \times 1, M \times M, M \times 1$, where M denotes the number of discrete node points along the microcell thickness direction. The input variable is the applied current I and the output is a $M \times 1$ vector that indicates ion concentration, C_e, at each node point.

Table 2
Governing equations for ETM.

Conservation equations
Ion conservation in electrode $\frac{\partial C_s}{\partial t} = \frac{D_s}{r^2}\frac{\partial}{\partial r}\left(r^2\frac{\partial C_s}{\partial r}\right)$
Ion conservation in electrolyte $\frac{\partial(\varepsilon_e C_e)}{\partial t} = \frac{\partial}{\partial x}\left(D_e^{eff}\frac{\partial}{\partial x}C_e\right) + \frac{1-t_+^0}{F}j^{Li}$
Charge conservation in electrode $\frac{\partial}{\partial x}\left(\sigma^{eff}\frac{\partial}{\partial x}\phi_s\right) - j^{Li} = 0$
Charge conservation in electrolyte $\frac{\partial}{\partial x}\left(\kappa^{eff}\frac{\partial}{\partial x}\phi_e\right) + \frac{\partial}{\partial x}\left(\kappa_D^{eff}\frac{\partial}{\partial x}\ln C_e\right) + j^{Li} = 0$
Electrochemical kinetics
Butler–Volmer equation $j^{Li} = a_s i_0\{\exp[\frac{\alpha_a F}{RT}\eta] - \exp[-\frac{\alpha_c F}{RT}\eta]\}$
$U_-(x) = -1.8636x^5 + 6.6478x^4 - 9.07126x^3 + 5.7843x^2 - 1.7970x + 0.3294$
$U_+(y) = -1550.039y^7 + 6806.298y^6 - 12633.679y^5 + 12829.327y^4 - 7687.388y^3 +$
Equilibrium potentials $2715.077y^2 - 523.437y + 46.682$
$x = C_{s,surf_-}/C_{s,\max_-}$
$y = C_{s,surf_+}/C_{s,\max_-}$

The state equation is transformed to a modal canonical form with:

$$\hat{A}_2 = \mathrm{diag}[\lambda_1 \quad \lambda_2 \quad \cdots \quad \lambda_M]$$

$$\hat{B}_2 = [1 \quad 1 \quad \cdots \quad 1]^T$$

$$\hat{C}_2 = [r_1\,\lambda_1\,r_2\,\lambda_2 \cdots r_M\,\lambda_M]$$

$$\hat{D}_2 = \left[Z + \sum_{k=1}^{n} \vec{r}_k\right] \tag{9}$$

where λ_k is the eigenvalues of the system matrix, A_2, Z is the steady state vector evaluated by $Z = -C_2A_2^{-1}B_2 + D_2$ and $\vec{r}_k$ is the residue vector obtained by:

$$\vec{r}_k = \frac{C_2\vec{q}_k\vec{p}_kB_2}{\lambda_k} \tag{10}$$

$\vec{q}_k$ and $\vec{p}_k$ denote the right and left eigenvectors of the system matrix A_2 and $A_2\vec{q}_k = \lambda_k\vec{q}_k$, $\vec{p}_kA_2 = \lambda_k\vec{p}_k$.

The *Mth* order system is reduced to the *Nth* order by grouping the residues according to the similarity of the eigenvalues [5]. The grouped residue vectors and the grouped eigenvalues are defined as:

$$\vec{r}_f = \sum_{k=k_{f-1}+1}^{k_f} \vec{r}_k$$

$$\lambda_f = \frac{\sum_{k=k_{f-1}+1}^{k_f} \lambda_k\vec{r}_k}{\vec{r}_f} \tag{11}$$

The *Nth* order state equation is constructed with the reduced matrices $A_2^*, B_2^*, C_2^*, D_2^*$ that have a dimension of $N \times N, N \times 1, M \times N, M \times 1$:

$$\mathrm{A}_2^* = \mathrm{diag}[\lambda_1 \quad \lambda_2 \quad \cdots \quad \lambda_N]$$

$$B_2^* = [1 \quad 1 \quad \cdots \quad 1]^T$$

$$C_2^* = [r_1\,\lambda_1\,r_2\,\lambda_2 \cdots r_N\,\lambda_N]$$

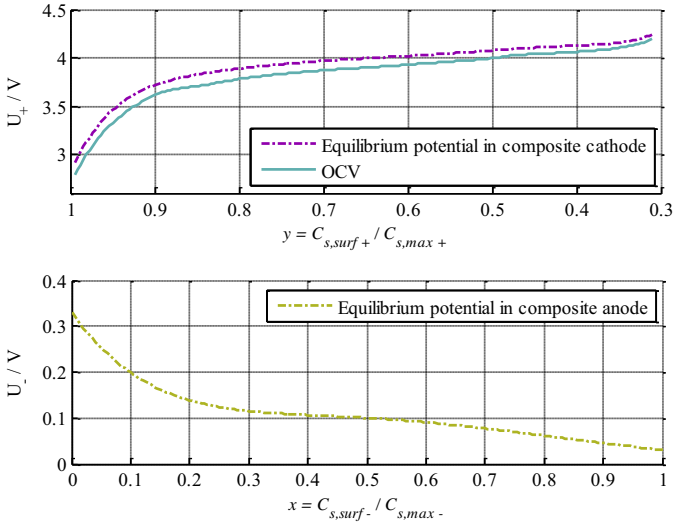

Fig. 3. The OCV curve obtained experimentally and the equilibrium potentials of electrodes.

$$D_2^* = \left[Z + \sum_{f=1}^{N} \vec{r}_f\right] \tag{12}$$

3.3. Potentials in electrodes and electrolytes

POD is a mathematical procedure that is used to find a basis for a modal decomposition of a data set. The data applied here is the rigorous solution of the potentials in electrode and electrolyte obtained by FEM. The governing equations for charge conservation in electrode and electrolyte are discretized and the resulting equations are expressed in the matrix form as follows:

$$A_3\vec{\phi} = b \tag{13}$$

where $\vec{\phi}$ is the FEM solution vector of the potentials at each grid points, A_3 and b denote the coefficients matrix and constant vector.

$\vec{\phi}$ can be approximated by a linear combination of the first N proper orthogonal modes (POMs) as shown in Eq. (14), where $\vec{\phi}_{appr}$ is the approximation solution, Φ is the POMs and a is the reduction variables.

$$\vec{\phi}_{appr} = \Phi \cdot \vec{a} \tag{14}$$

The POMs are the eigenvectors obtained by singular value decomposition of the discrete kernel given by $\vec{\kappa} = \vec{\phi}^T \cdot \vec{\phi}$ and sorted in a manner that the corresponding eigenvalues are in a non-increasing order, as shown in Eq. (15). Σ is the diagonal matrix of eigenvalues and N denotes the model order that we applied in POD.

$$[U\Sigma V] = svd(\vec{\phi}_{\mathrm{full}}^{\,T} \times \vec{\phi}_{\mathrm{full}}) \qquad \Phi = \mathrm{U}(:, 1:\mathrm{N})$$

The reduction variables, $\vec{a}$, are solved by substituting Eq. (14) into Eq. (13), which yields Eq. (16):

$$A_3(\Phi \cdot \vec{a}) = b \;\Rightarrow\; \vec{a} = \Phi^T A_3^{-1} b \tag{16}$$

Table 3
Low orders Padé approximation of $C_{s,surf}$.

Order	Padé approximation
2nd	$\dfrac{-\frac{3D_s m}{R_s} - \frac{2mR_s s}{7}}{s + \frac{R_s^2 s^2}{35D_s}}$
3rd	$\dfrac{-\frac{3D_s m}{R_s} - \frac{4mR_s s}{11} - \frac{mR_s^2 s^2}{165D_s}}{s + \frac{3R_s^2 s^2}{55D_s} + \frac{R_s^4 s^3}{3465D_s^2}}$
4th	$\dfrac{-\frac{3D_s m}{R_s} - \frac{2mR_s s}{5} - \frac{2mR_s^3 s^2}{195D_s} - \frac{4mR_s^5 s^3}{75075D_s^2}}{s + \frac{R_s^2 s^2}{15D_s} + \frac{2R_s^4 s^3}{2275D_s^2} + \frac{R_s^6 s^4}{675675D_s^3}}$
5th	$\dfrac{-\frac{3D_s m}{R_s} - \frac{8mR_s s}{19} - \frac{21mR_s^3 s^2}{1615D_s} - \frac{4mR_s^5 s^3}{33915D_s^2} - \frac{mR_s^7 s^4}{3968055D_s^3}}{s + \frac{7R_s^2 s^2}{95D_s} + \frac{3R_s^4 s^3}{2261D_s^2} + \frac{2R_s^6 s^4}{305235D_s^3} + \frac{R_s^8 s^5}{218263025D_s^4}}$

The selected POMs form a basis that facilitates to capture the dominant characteristics of the system dynamics and enables representation of the most significant information of the variables under various circumstances. In this work, the potential data set $\vec{\phi}$ used to build the kernel $\vec{\kappa}$ is evaluated under 1 C discharge condition with uniform current density.

3.4. Electrochemical kinetics

Electrochemical reactions that take place at the interface between electrodes and electrolytes are described by the Butler–Volmer equation. The nonlinear functions are linearized based on the fact that the overpotentials vary within a linear range under normal operating conditions [4].

$$j^{Li} = a_s i_0 \frac{(\alpha_a + \alpha_c)F}{RT}\eta \tag{17}$$

4. Analysis of sub-models performances

Performances of the sub-models are analyzed by comparing the models before and after reduction. The model before the reduction is numerically solved using the finite element method (FEM), where the number of grids in the radial direction of particles and thickness direction of the cell are 25 and 15, respectively. The three variables, $C_{s,surf}$, C_e and ϕ are used to evaluate performances of the sub-models.

4.1. Order reduction for ion concentration in electrode particles

Since the average concentration in electrode particles, $C_{s,ave}$, is easily obtained by the volume average equation, only the surface concentration, $C_{s,surf}$, is the crucial variable to be considered for the evaluation of performances with respect to frequency, time and static response. The response of $C_{s,surf}$ at a current density, j^{Li}, can be formulated by different methods including parabolic, quartic polynomial and the Padé approximation. The transfer functions reformulated from a parabolic and a quartic profile are shown in Eq. (18) [10].

$$\begin{aligned}
\frac{C_{s,surf}(s)}{j^{Li}(s)} &= -\frac{15mD_s + R_s^2 ms}{5R_s s}\ \text{parabolic}\\
\frac{C_{s,surf}(s)}{j^{Li}(s)} &= -\frac{3150D_s^2 m + 315D_s mR_s^2 s + mR_s^4 s^2}{35R_s s(R_s^2 s + 30D_s)}\ \text{quartic}\\
\text{where} m &= \frac{1}{a_s F D_s}
\end{aligned} \tag{18}$$

Frequency responses of the analytical exact solution given in Eq. (1), the two different polynomial approaches and the Padé approximation from the 2nd to 10th order with a step of a two-order for surface concentration of particles on the anode side are plotted in Fig. 4. Comparison between the analytical solution and the two approximation methods shows that the Padé approximation approaches the analytical exact solution up to a certain frequency that depending upon the order. The higher the order is, the smaller the difference of the responses in magnitude and phase. In addition, the range of the response of the 4th order Padé approximation is comparable to that of the quartic polynomial. Conversely, the parabolic polynomial only works over the range of very low frequencies, which means that the dynamic performance is of less satisfactory. The quartic profile with an extra state better represents its response over a high frequency range, but it is hard to extend the order of polynomial systematically to meet the accuracy requirements.Time responses of $C_{s,surf}$ by applying different methods at AC currents are compared in Fig. 5. Relative errors are calculated in percentage, which are shown in Eq. (19), where $\hat{y}_i$ is the simulation data of the different methods, and y_i is the FEM solution with 25 grid points on radial direction (or experimental data). The parabolic method is not considered because of its large error.

$$\text{Relative error} = \left(\frac{\hat{y}_i - y_i}{y_i}\right) \times 100\% \tag{19}$$

The 2nd order of the Padé approximation (yellow dot-dashed line) shows the largest discrepancy in magnitude and phase compared to the FEM solution. The quartic profile (purple dashed line) shows improved tracking behavior, while the 6th order of the Padé approximation (green line) has the closest match to the FEM solution. The time responses shown in Fig. 5 verify the results of the frequency responses as shown in Fig. 4 where the Padé approximation can best represent the FEM solution over a wide frequency range if an appropriate order is determined.

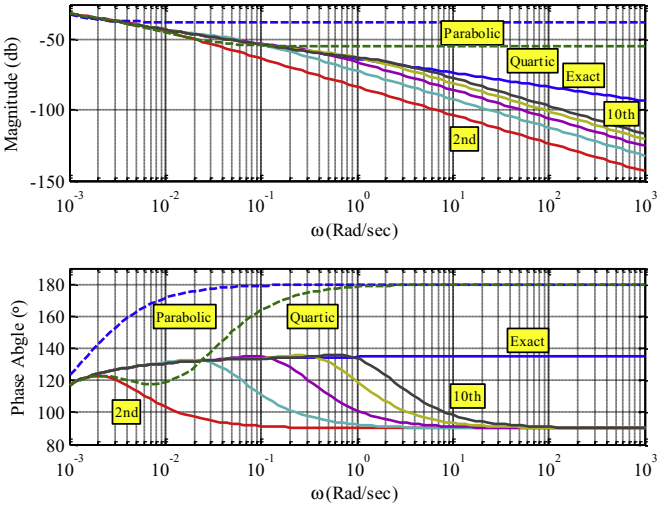

Fig. 4. Frequency responses of the surface concentration of a particle on the anode side: analytical exact solution, parabolic and quartic polynomial and the different order of Padé approximation.

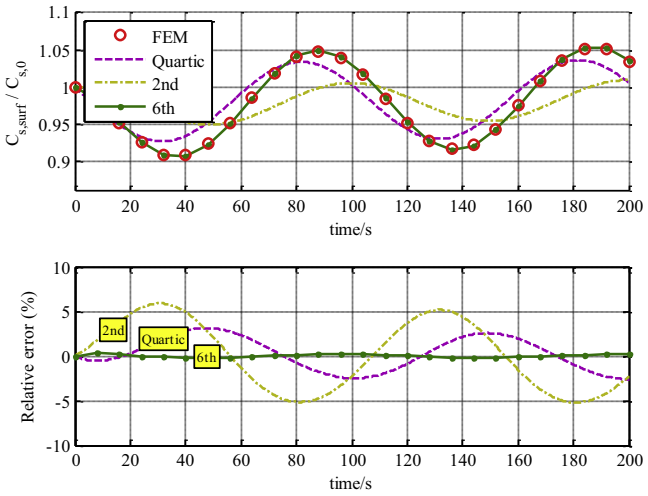

Fig. 5. Time responses of surface concentration of a particle on anode: FEM, quartic polynomial, and 2nd and 6th order of the Padé approximation.

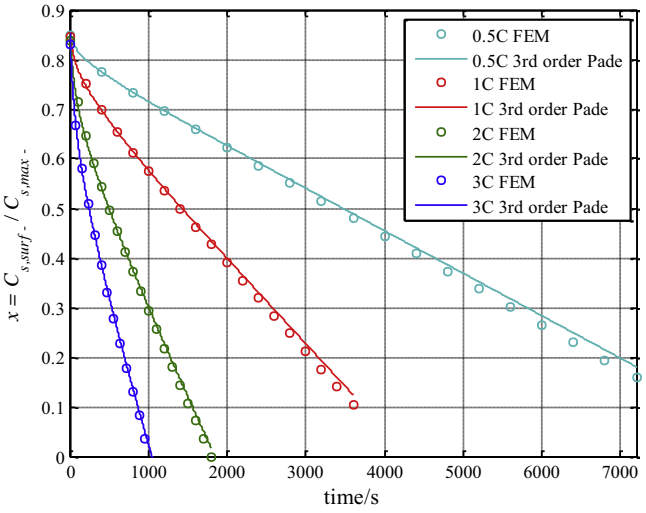

Fig. 6. Stoichiometry number of the anode during full discharge: 0.5 C, 1 C, 2 C and 3 C rate.

One other criterion for assessments is the accuracy of the surface concentration at steady state. According to the analysis in Fig. 4, the 3rd order Padé approximation should be enough to represent steady state or low frequency behavior of variables. Simulation results of the stoichiometry number in the anode side during the discharging process at different C rates are depicted in Fig. 6, where the stoichiometry number is a function of surface concentration that is defined as $x = C_{s,surf\_}/C_{s,\max\_}$ and is used to determine the equilibrium potential in the anode. The results obtained by the 3rd order Padé approximation are compared to those given by FEM (circles), which shows that the 3rd order Padé approximation is accurate enough to replace the FEM method in the steady state. The model order should be determined by balancing the accuracy and the computational time [14].

4.2. Order reduction for ion concentration in electrolyte

The 3rd order of residue grouping (RG) method is employed to replace the FEM method for calculation of ion concentrations in the electrolyte. Distributions of ion concentrations using RG and FEM at various time instants are plotted in Fig. 7, where the battery is discharged from 100% SOC with 1 C rate. The x and y coordinates represent dimensionless thickness and ion concentration,

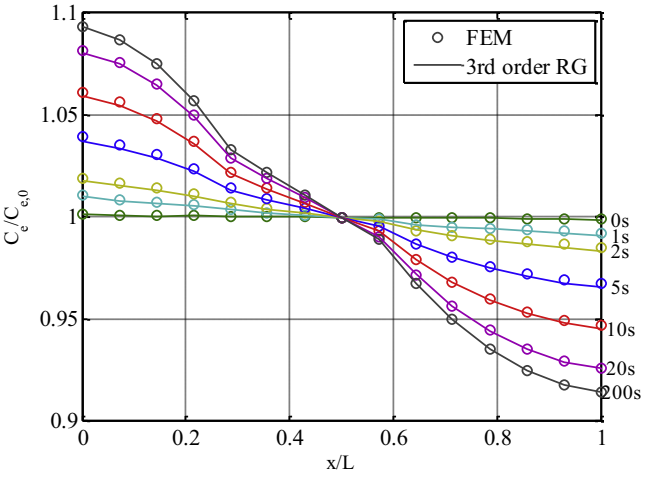

Fig. 7. Ion concentration in the electrolyte at various times during 1 C discharge.

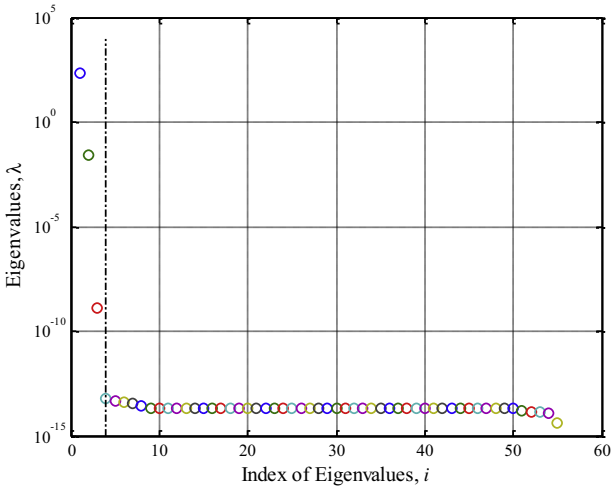

Fig. 8. Eigenvalue spectrum of the potential data set obtained from the model with FEM during discharge at 1 C rate.

respectively. The nominated $C_e/C_{e,0}$ with circles are the concentrations calculated by FEM at each grid point across the cell and those with solid lines are calculated by the 3rd order RG sub-model. With uniform current density applied, the results show that the RG method can follow the response of FEM with a decent accuracy, which can be further improved by appropriately adjusting the upper and lower limits of each eigenvalue group.

4.3. Order reduction for potentials in electrode and electrolyte

POD is employed to reduce the order for potentials. To determine the order for POD, eigenvalue spectrum of the discrete kernel, $\vec{\kappa} = \vec{\phi}_{full}T \cdot \vec{\phi}_{full}$, is calculated and plotted in Fig. 8, where the eigenvalues, λ_i are the diagonal elements of matrix Σ in Eq. (15). The results show that the magnitude rapidly decreases for the first four eigenvalues and then remains a small constant value. Since the importance of the POMs is denoted by the corresponding eigenvalues, the first 4 POMs can represent the most significant dynamic characteristics of the system. As a result, the basis of the POD can be determined by considering the eigenvalue spectrum, and a linear combination of the selected POMs is used to construct a reduced model for potentials in electrode and electrolyte. In this case, a 3rd order sub-model is employed.

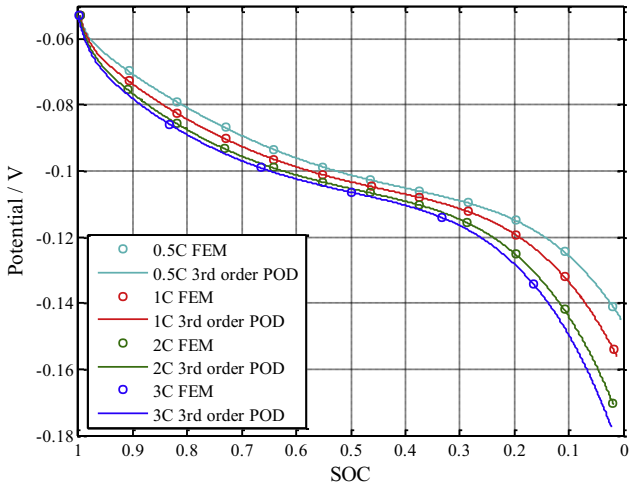

Fig. 9. Electrolyte potential in the center of the cell during discharging with 1 C rate.

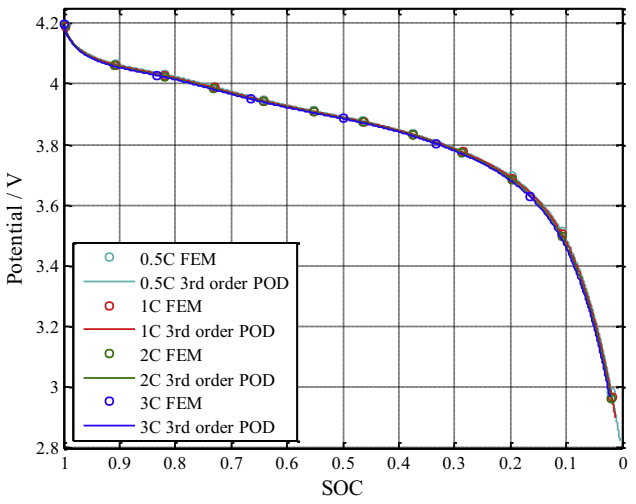

Fig. 10. Electrode potential at the interface between separator and composite cathode during discharge with 1 C rate.

To assess performance of the 3rd order POD sub-model, potentials in electrode and electrolyte calculated by reduced order sub-models are compared to those of FEM in Figs. 9 and 10, where the battery is discharged with 0.5 C, 1 C, 2 C and 3 C rate from 100% down to 0% SOC.

Since the data produced by the reduced sub-model and FEM results are hard to compare using a 3D surface plot, only two variables at representative grid points are selected to access the accuracy of the calculations. Variation of the electrolyte potential in the middle of the cell is shown in Fig. 9, where the negative value of potential is caused by the zero potential refference that is set at the anode boundary near the current collector. The electrode potential at the cathode-separator interface point is also given in Fig. 10.

Comparison shows that the responses of the 3rd order of POD sub-model (solid curves) are comparable to those of the FEM (circles) that has 15 grid points along the thickness direction including three grid points on the separator. The proposing method allows for substantial reduction of the matrix size of the potential from 27×27 to 3×3, so that the computational time can be significantly reduced while maintaining the accuracy.

5. ROM for a single cell

ROM for a single cell is constructed by the sub-models. A schematic diagram for the integrated ROM is shown in Fig. 11, where input variables are load profiles along with ambient temperature that can be constant current (CC) or constant voltage (CV) charging and discharging. The data set for potential φ is calculated offline using FEM and then stored for POD. Parameters used for these specific cells are listed in the appendix. Order for sub-models is defined as an extra input parameter that can be determined upon required accuracy. System matrices for each sub-model is determined based on parameters, initial and boundary conditions, and stored prior to the main loop.

The main loop consists of three sub-models. Ion concentrations are firstly solved with uniform current density, the resulting state variables $C_{s,surf}$, $C_{s,ave}$ and C_e are used to determine the equilibrium potential, SOC and diffusion term in charge conservation equations correspondingly. Then the potentials are calculated based on the ion concentrations at the instants.

The output variables are terminal voltage or current, ion concentrations, SOC and other internal variables.

5.1. Effects of sampling time

Sampling time is one of the crucial factors for the determination of hardware. A short sampling time can overload hardware and increase its overall costs, particularly when a large number of cells are connected in series and parallel. Therefore, computational time and error of terminal voltage is calculated as a function of sampling times and plotted in Fig. 12, where the initial SOC of the battery was 100% and the battery was discharged with 1 C rate. The model is coded with MATLAB and runs on PC with 3.4 GHz processor, whereas execution time is measured. The errors are normalized as below, where $\hat{y}_i$ and y_i are the data obtained from simulations and experiments and n is the number of sampling points.

$$\text{Normalized error} = \sqrt{\frac{\sum (\hat{y}_i - y_i)^2}{n}} \tag{20}$$

The blue line with stars and green line with points denote the computational time and errors, respectively. As expected, the errors are reciprocal proportional to the computational time. An optimal sampling time can be determined by considering time and accuracy. We chose about 1 second as the optimal sampling time, where the curves cross.

5.2. Experimental validation of the ROM

The constructed ROM is validated against experimental data collected from a test station that was constructed with a programmable power supply and an electronics load that are controlled by LabVIEW. The cells used for this validation are pouch type lithium polymer batteries, whose specifications are listed below.

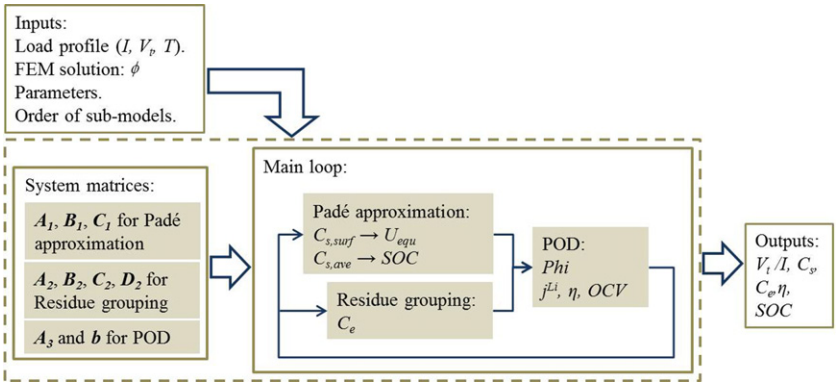

Fig. 11. Schematic diagram for the ROM for a single cell.

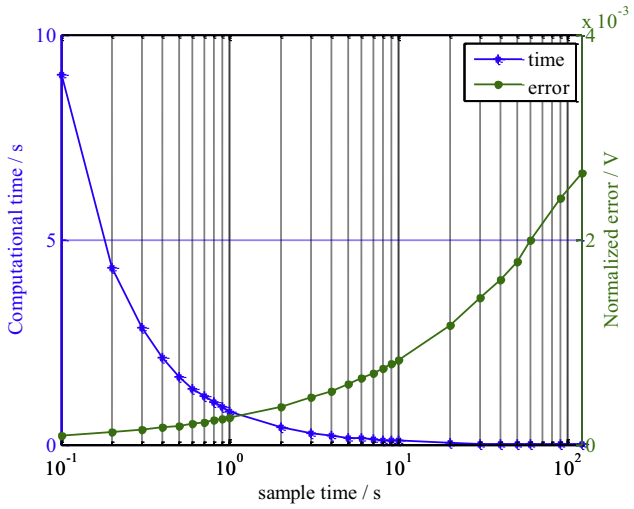

Fig. 12. Computational time and error with respect to different sample rate.

Chemistry: Cathode, $LiMn_2O_4$ (spinel); Anode, surface modified graphite; Electrolyte, Gel polymer ($LiPF_6$ + EC/DEC/EMC); Separator, Ceramic coated separator.

Dimension: 14.7mm × 280mm × 185 mm.

Nominal capacity: 50 Ah.

Operation range of the terminal voltage: 2.7 V–4.2 V.

The experimental data are acquired under constant temperature at 25 °C by using an extra thermal chamber and with different current loads that include full charge and full discharge with constant current at 0.5, 1, 2 C, 3 C rate, continuously charging and discharging multiple cycles and a current profile obtained from a driving cycles of an electric vehicle. Since the nominal capacity of the large format lithium ion battery tested in this work is 50 Ah, which is relatively high compared to other pouch type batteries, the ROM was validated up to 3 C. For continuous charging and discharging at higher C-rate, severe heat generation caused by large current will accelerate the battery degradation and result in changes of physical parameters in the ROM, which obstacle the validation of the model.

5.2.1. Discharging and charging

Terminal voltage V_t between simulation results of ROM (solid line) and experimental data (circles) are plotted in Figs. 13 and 14,

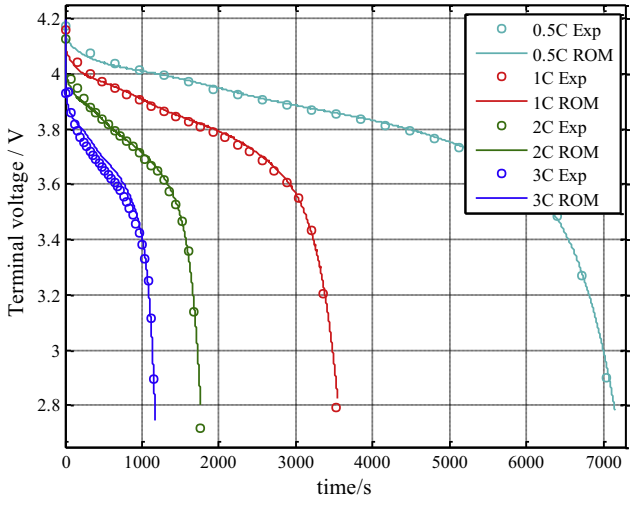

Fig. 13. Comparison of terminal voltage from simulation and experiments during 0.5 C, 1 C, 2 C and 3 C discharge.

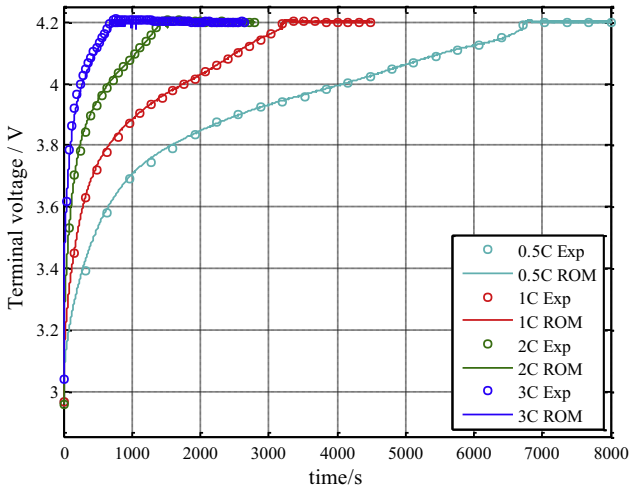

Fig. 14. Comparison of terminal voltage from simulation and experiments during 0.5 C, 1 C, 2 C and 3 C charge.

where the simulation results of ROM have a fairly good match with the experimental data at different current rates.

The percentage of relative errors defined in Eq. (19) during discharging and charging are plotted in Fig. 15. Overall errors are less than 2% except at the end of charging and the beginning of discharging where the SOC is relatively low. The error is caused by the simplified equation for the overpotential since the terminal voltage is the difference between the OCV and the overpotential that becomes large at low SOC range.

5.2.2. Multiple cycles and EV driving cycle

Long term stability of the ROM is assessed by the response of terminal voltage at multiple cycles and an EV driving cycle. The multiple cycles consist of a combination of CC/CV charging and CC discharging with various current amplitudes. Simulation results of the ROM are compared to the experimental data in Figs. 16 and 17. There are some transient errors appeared at the instant when an abrupt current change occurs, which is caused by inaccurate determination of equilibrium potential that is a function of surface concentration as shown in Table 2. In fact, the surface concentration in electrode particle is estimated by 3rd order Padé approximation, which is accurate enough to represent the static responses as shown in Fig. 6, but is inadequate to capture the high

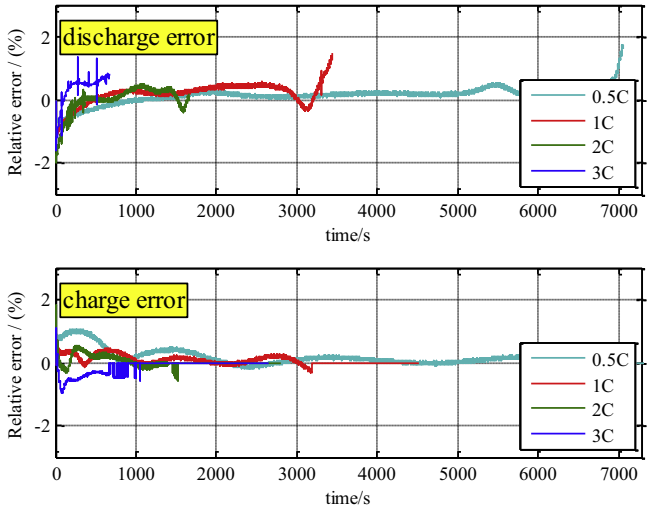

Fig. 15. Percentage errors of the terminal voltage at discharge and charge.

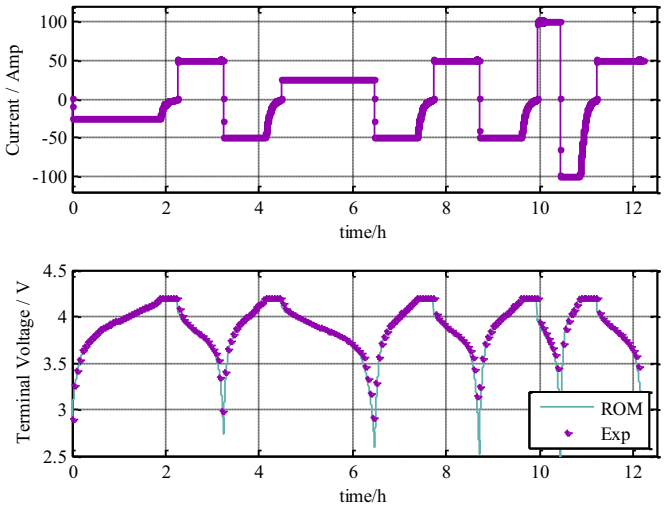

Fig. 16. Comparison of terminal voltage between simulation and experiments at multiple charging and discharging cycles.

frequency dynamics presented in driving cycles. Since the order of the Padé approximation is systematically adjustable unlike the polynomial approach, the accuracy of ROM can be further improved by increasing the order of the approximation, which leads to high computational expense.

5.2.3. Comparison with the ROM developed previously

Two major features of the newly developed ROM are compared with those of the previously developed ROM, which include computational time and normalized voltage errors as a function of the sampling time, as plotted in Fig. 18. The computational time is significantly reduced for the sampling time that is less than 1 sec while the errors of terminal voltage are almost the same until 70 sec, but are less after 70 sec.

Finally, execution time of three models including the time required for calculation of sub-models is listed in Table 4. The time analysis was carried out using the MATLAB profiler and the individual term was calculated based on the execution time of each sub-model functions. The ROM proposed in this paper needs the shortest time and reduces the computation time to one tenth of the previous ROM.

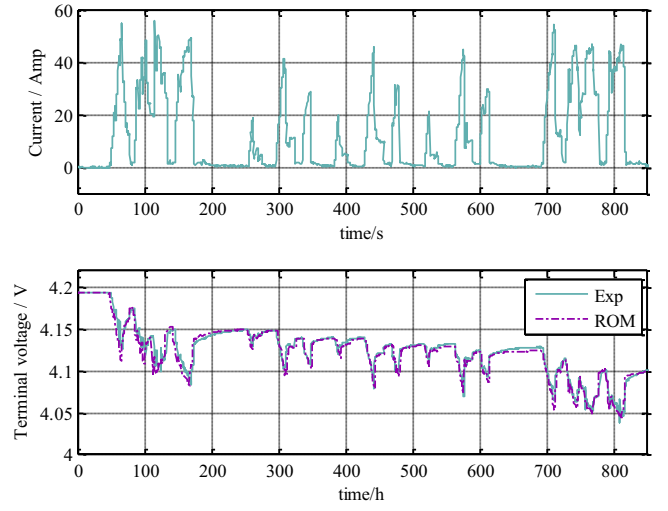

Fig. 17. Comparison of terminal voltage from simulation and experiments at a current profile measured at an EV driving cycle.

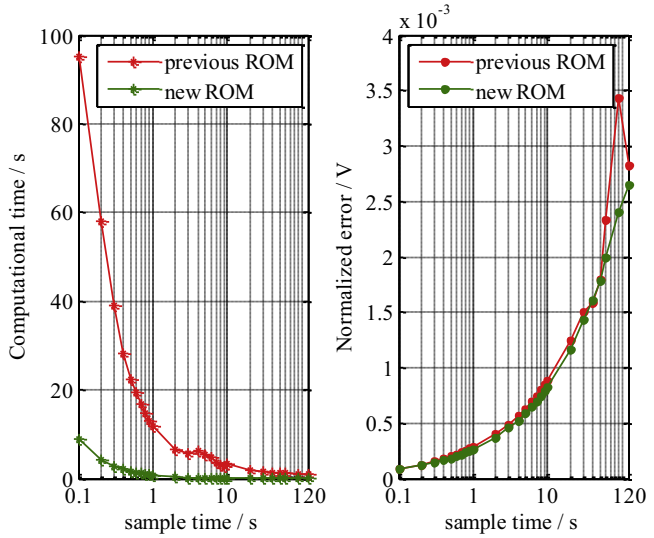

Fig. 18. Comparison of computational time and error vs. sample time between the previous ROM [14] and the new proposing ROM.

Table 4
Comparison of computational time (second) between previous ROM and the new approach.

	Previous ROM [14]	New ROM
Total	10.09	1.05
C_s	6.05	0.08
C_e	0.05	0.03
Phi	3.36	0.34
Others	0.63	0.6

6. Conclusion

Electric equivalent circuit models have been widely used for algorithms of SOXs embedded in BMS, but have limitations because of the absence of the physical phenomena that take place in batteries. ROM based on electrochemical principles can provide a potential solution that allows for monitoring internal physical variables. As a result, advanced control algorithms can be designed based on these variables. In fact, hundreds of cells are needed for high power systems, where the computational time of the model is one of impeding factors for implementations on microcontrollers.

This paper proposed a ROM that is constructed by integration of sub-models derived using different order reduction techniques. The diffusion in solid is simplified by Padé approximation, while the concentration in electrolyte is reduced by applying the residue grouping method. In addition, POD is adopted to shrink the matrix size for potentials. The integrated ROM is then validated against experimental data at various operating conditions. Main accomplishments and findings are summarized as follows:

- Comparative analysis of the performances of the individual reduced sub-models in time and frequency domain,
- Selection of sampling time based on errors,
- Performance of the developed ROM
  - Reduction of computational time to one-tenth of the previous ROM while the accuracy remains the same or better than the previous ROM regardless of the sampling time.
  - The order is adjustable dependent upon input profiles or accuracy requirements.

Future work will include development and integration of the degradation model. In addition, the accuracy of the model in real time operation will be improved using advanced control methods.

References

[1] L. Gao, S. Liu, R.A. Dougal, IEEE Trans. Components Packaging Technol. 25 (3) (2002) 495–505.
[2] M. Doyle, T.F. Fuller, J. Newman, J. Electrochemical Soc. 140 (6) (1993) 1526–1533..
[3] K.A. Smith, C.D. Rahn, C.Y. Wang, Energy Convers. Manage. 48 (9) (2007) 2565–2578.
[4] M. Xiao, S.Y. Choe, J. Power Sources 218 (2012) 357–367.
[5] K.A. Smith, C.D. Rahn, C.Y. Wang, J. Dyn. Sys. Meas. Control 130 (1) (2008) 11012.
[6] L. Cai, R.E. White, J. Electrochemical Soc. 156 (3) (2009) A154–A161.
[7] C.Y. Wang, W.B. Gu, B.Y. Liaw, J. Electrochemical Soc. 145 (10) (1998) 3407–3417.
[8] V.R. Subramanian, V.D. Diwakar, D. Tapriyal, J. Electrochemical Soc. 152 (10) (2005) A2002–A2008.
[9] S. Liu, Solid State Ionics 177 (1) (2006) 53–58.
[10] V. Ramadesigan, V. Boovaragavan, J.C. Pirkle Jr., V.R. Subramanian, J. Electrochemical Soc. 157 (7) (2010) A854–A860.
[11] T.S. Dao, C.P. Vyasarayani, J. McPhee, J. Power Sources 198 (2012) 329–337.
[12] J.C. Forman, S. Bashash, J.L. Stein, H.K. Fathy, J. Electrochemical Soc. 158 (2) (2011) A93–A101.
[13] T. Jacobsen, K. West, Electrochimica acta 40 (2) (1995) 255–262.
[14] X. Li, M. Xiao, S.Y. Choe, Electrochimica Acta 97 (2013) 66–78.
[15] Y. Zhao, S.Y. Choe, SAE Technical Paper, 2014-01-1835 (2014) .